




# Improved porosity promotes reendothelialization and smooth muscle remodeling in decellularized tissue-engineered vascular grafts

Tun Wang<sup>a,b,1</sup>, Sheng Liao<sup>a,b,1</sup>, Peng Lu<sup>a,b</sup>, Zhenyu He<sup>a,b</sup>, Siyuan Cheng<sup>a,b</sup>, Tianjian Wang<sup>a,b</sup>, Zibo Cheng<sup>a,b</sup>, Yangyang An<sup>a,b</sup>, Mo Wang<sup>a,b</sup>, Chang Shu<sup>a,b,c,\*</sup> 

<sup>a</sup> Department of Vascular Surgery, The Second Xiangya Hospital, Central South University, Changsha, 410011, China

<sup>b</sup> Institute of Vascular Diseases, Central South University, Changsha, 410011, China

<sup>c</sup> Center of Vascular Surgery, Fuwai Hospital, Chinese Academy of Medical Sciences and Peking Union Medical College, Beijing, 100037, China

## ARTICLE INFO

### Keywords:

Tissue-engineered vascular graft  
Reendothelialization  
Remodeling  
Arteriovenous graft  
Hemodialysis

## ABSTRACT

Decellularized tissue-engineered vascular grafts (dTEVGs) exhibit superior biocompatibility, anti-infection properties and repair potential, contributing to better patency and making them a more ideal choice for arteriovenous grafts (AVGs) in hemodialysis compared to chemically synthesized grafts. However, the unsatisfactory reendothelialization and smooth muscle remodeling of current dTEVGs limit their advantages. In this study, we investigated the use of elastase to improve the porosity of elastic fiber layers in dTEVGs, aiming to promote cell infiltration and achieve superior reendothelialization and smooth muscle remodeling. Our findings revealed that elastase treatment induced scattered cracks and holes in the elastic fiber layers of dTEVGs. Porous dTEVGs demonstrated increased cell infiltration in rat subcutaneous tissue. In the rat AVG models, mildly elastase-treated dTEVGs significantly improved cell infiltration and graft remodeling, including adequate smooth muscle cell (SMC) repopulation, impressive reendothelialization and regeneration of the extracellular matrix, without stenosis, dilation or disintegration of the grafts. This study demonstrates that porous dTEVGs promote reendothelialization, smooth muscle remodeling and extracellular matrix regeneration while retaining a stable graft structure, enhancing durability and puncture resistance in hemodialysis.

## 1. Introduction

Chronic kidney disease (CKD), a progressive reduction of kidney function, leads to irreversible nephron loss, end-stage renal disease (ESRD) and premature death [1–3]. The global burden of chronic kidney disease has continued to grow in the past 30 years, with prevalence rate increasing 29.3 % and mortality rate increasing 41.5 % [4]. With the destruction of structure and function of kidney, CKD patients will develop ESRD, which needs renal replacement therapy [5]. Hemodialysis is the most prevalent renal replacement therapy for patients with ESRD, and hemodialysis access is crucial to provide adequate hemodialysis and keep patients alive [6]. For many patients without access to arteriovenous fistulas, the arteriovenous graft (AVG) is the optimal choice [7–10].

Expanded polytetrafluoroethylene (ePTFE) graft, a chemically

synthetic vascular graft, is the most used vascular graft in clinic. However, lack of cell regeneration, ePTFE grafts have drawbacks of easy infection, unsatisfactory patency, lack of functional endothelium, and lack of structure repair during repeated puncture in hemodialysis [11–13]. Developing superior materials for vascular grafts is needed. Decellularized tissue-engineered vascular grafts (dTEVGs) are natural blood vessels with cellular components removed and structure and properties of extracellular matrix components retained, leading to good biocompatibility and low immunogenicity [14–19]. An ideal dTEVG has the ability to support host cell growth and interaction between cells, and regenerate to a biological living vessel, similar to the native vessel [13, 14, 18, 20]. Some dTEVGs have been attempted for AVGs. Studies have shown that compared to ePTFE grafts, dTEVGs have better patency with a lower infection rate as AVGs [21–23].

However, studies show that the cell infiltration and remodeling of

\* Corresponding author. Department of Vascular Surgery, The Second Xiangya Hospital, Central South University, Changsha 410011, China. Institute of Vascular Diseases, Central South University, Changsha 410011, China. Center of Vascular Surgery, Fuwai Hospital, Chinese Academy of Medical Sciences and Peking Union Medical College, Beijing 100037, China.

E-mail address: [Changshu\\_vascular@163.com](mailto:Changshu_vascular@163.com) (C. Shu).

<sup>1</sup> These authors contribute equally to this work as co-first authors

<https://doi.org/10.1016/j.mtbio.2024.101402>

Received 9 September 2024; Received in revised form 6 December 2024; Accepted 10 December 2024

Available online 12 December 2024

2590-0064/© 2024 The Authors. Published by Elsevier Ltd. This is an open access article under the CC BY-NC-ND license (<http://creativecommons.org/licenses/by-nc-nd/4.0/>).

dTEVGs are not as ideal as expected, with insufficient recellularization and reendothelialization, lack of effective formation of the smooth muscle layer or endothelium [24–26]. Sufficient cell infiltration and remodeling is crucial for dTEVGs to restore their biological function in hemodialysis, because they are subjected to repeated and long-term needle puncture, which may lead to rupture, pseudoaneurysm, thrombosis, stenosis and increased infection risk in the grafts [13]. Cell infiltration is the first step of graft remodeling. However, the dense matrix of dTEVGs, such as the elastic fiber layers, prevents cell infiltration and suppresses remodeling, limiting a further use of dTEVGs in hemodialysis [27,28]. Limited evidences have shown increasing the porosity of the dense structure of dTEVGs increased the cell infiltration [25,29–32]. However, it remains unclear whether increasing the porosity of the elastic fiber layers in dTEVGs promotes the cell infiltration and even subsequent vascular remodeling when used as AVGs. Innovatively, we use mild elastase treatment to increase the porosity of elastic fiber layers in the dTEVGs as hemodialysis access of the rat models, achieving impressive remodeling, with smooth muscle layer regeneration, reendothelialization and secretion of extracellular matrix.

## 2. Method

### 2.1. Decellularization of rat carotid arteries

The right rat carotid arteries (CAs) (approximately 1.5 cm) from 11-week-old male Sprague-Dawley (SD) rats were dissected and removed using sterile techniques. Decellularization was performed following previously reported procedures [33–36]. Briefly, the CA was placed in a  $-20^{\circ}\text{C}$  freezer overnight. After thawing, the CA was incubated in CHAPS buffer (8 mM CHAPS, 1 M NaCl and 25 mM EDTA in PBS) for 12 h, followed by a 60-min wash with PBS. Subsequently, the CA was incubated for 24 h in sodium dodecyl sulfate buffer (1.8 mM sodium dodecyl sulfate, 1 M NaCl and 25 mM EDTA in PBS). To thoroughly remove the detergent, the CA was washed with PBS for 24 h. To further eliminate nucleic acid macromolecules, the CA was incubated in PBS containing DNase I (3000 U/ml) and RNase A (3000 U/ml) at room temperature for 1 h, with a subsequent 60-min wash with PBS. The decellularized CA was stored at  $4^{\circ}\text{C}$  in PBS with penicillin (100 U/ml) and streptomycin (100 mg/ml) until used.

### 2.2. Elastase treatment of decellularized carotid arteries

Decellularized CAs were incubated in PBS containing elastase (20 mg/ml, Fushen, FS1140, diluted 120 times before use) in  $37^{\circ}\text{C}$  water bath for 15, 30 and 45 min, respectively. The control group was incubated in PBS. Subsequently, all decellularized CAs were washed with PBS for 60 min to fully remove residual elastase prior to use (Fig S1). Fresh elastase-treated decellularized CAs were used in related experiments.

### 2.3. Scanning electron microscope

The decellularized CAs with or without elastase treatment were lyophilized for 24 h to dehydrate them. They were then mounted onto aluminum stubs. After adequate sputter-coated with gold, these samples were observed using a scanning electron microscope (SEM) (Phenom Pro, Phenom-World BV, Eindhoven, the Netherlands).

### 2.4. Subcutaneous implantation

The animal use protocols described below have been approved by the Institutional Animal Care and Use Committee (IACUC) in The Second Xiangya Hospital of Central South University (Approval No. 20240608). All experiments were performed in accordance with the National Institutes of Health Guide for the Care and Use of Laboratory Animals. Elastase-treated decellularized CAs (15, 30, and 45 min) and the control

samples were inserted with tubes, with both ends of the grafts closed using 8-0 silk sutures to evaluate cell infiltration from the grafts' outer side [37]. Following previous research, these samples were implanted into the subcutaneous tissue of the male SD rats ( $n = 3$ , 11 weeks), with isoflurane (RWD, China) used for anesthesia. Briefly, four symmetrical 1 cm wide skin incisions were made on the back of the rat [28,29]. Blunt dissection was then used to create four subcutaneous pouches in each rat. Each sample was placed into each subcutaneous pouch and the incisions were closed with 3-0 silk sutures. After 21 days, the samples were extirpated, and the rats were sacrificed.

### 2.5. Construction of rat arteriovenous graft models

The renal failure rat carotid artery-jugular vein AVG model requires a high level of technical skill and microvascular surgical expertise [33]. It is strongly recommended that the surgical procedures are performed by at least one trained surgeon. The surgical procedure was based on a previous study [33]. Due to the smaller diameters of the carotid arteries and jugular veins in young SD rats, which makes prolonged surgeries more difficult, 11-week-old male SD rats were selected for the model. After preparing 15-min, 30-min, and 45-min elastase treatments as well as non-treatment controls, decellularized CAs were placed between the carotid arteries and jugular veins. Non-invasive doppler ultrasound was employed to monitor vascular patency, hemodynamics and change of inner diameter in the model at Days 7, 21 and 42 post-surgeries, until the rats were sacrificed. The inner diameters of grafts were measured to monitor whether the stenosis, dilation, aneurysm or disintegration occurred ( $n = 4$ ). More details can be found in the previous study [33].

### 2.6. Histology

Immediately after tissue removal, specimens were rinsed with PBS. Fresh specimens were fixed in 4 % paraformaldehyde. Following dehydration with ethanol and xylene, the specimens were embedded in paraffin and were cut into  $4.0\ \mu\text{m}$  cross sections. Hematoxylin and eosin (H&E) staining was employed to assess the histomorphology and cell infiltration (Servicebio, G1005). Elastic Van Gieson (EVG) staining was utilized to evaluate the integrity and crack of elastic fibers, assessing the effect of elastase (Hao Ke Biotechnology Co. Ltd, HKT2034). Masson's trichrome staining was employed to measure the collagen area of the grafts and assess the structural deformation (Solarbio Life Sciences, G1340). The collagen proportion of grafts were also measured using Masson's trichrome staining. Herovici's staining was used to differentiate the young and mature collagen in the grafts (Biorbyt, orb1711404). Picrosirius red staining was utilized to identify different collagen types (Solarbio, G1472).

### 2.7. Immunofluorescence

After deparaffinization, tissue sections underwent antigen retrieval by heating in citric acid buffer ( $\text{pH} = 6.0$ ) at  $100^{\circ}\text{C}$  for 15 min. To block antigens, 5 % bovine serum albumin was applied for 60 min at room temperature. The sections were then incubated with primary antibody at  $4^{\circ}\text{C}$  overnight. In this study, the following primary antibodies were used: anti-CD31 antibody (Abcam, ab222783, 1:100), anti-CD68 antibody (Abcam, ab31630, 1:100), anti- $\alpha$ -SMA antibody (Abcam, ab7817, 1:100), anti-CNN1 antibody (CST, 17819S, 1:100), anti-Collagen I antibody (Servicebio, GB11022, 1:400), anti-Collagen III antibody (Servicebio, GB111629, 1:400), anti-CD45 antibody (Abclonal, A2115, 1:100), anti-Vimentin antibody (Servicebio, GB111308, 1:100). After incubation overnight, the sections were treated with Alexa Fluoro secondary antibodies for 1 h and then stained with DAPI (P36935, Invitrogen) to visualize cell nuclei. Positively staining cells were counted under high power fields. IgG isotype, negative tissue and endogenous tissue background served as antibody negative controls.

## 2.8. Counting of infiltration cells

To clearly visualize the site of cell infiltration during immunofluorescence staining, tissue autofluorescence was moderately exposed to highlight the graft structure. Cells within the graft were counted as infiltrated cells. At least three sections of the same sample were taken, at least three high-power fields per section were taken, and the data were obtained from at least three samples for analysis. Because there was too little CD68-positive cell infiltration in the AVG model, all CD68-positive cells in the entire graft were counted.

## 2.9. Quantification of area and proportion

The area and proportion were quantified using ImageJ (Version 1.52a). In vitro, the deformation of graft cross sections was assessed by the increase of the blue area in Masson's trichrome staining. To quantify the dilation of the grafts in the AVG models, the sections of decellularized, elastase-treated and implanted grafts were stained with H&E staining. The perimeters of the lumen were calculated and compared. Considering that the presence or absence of blood flow in vivo or in vitro affects the luminal area of the graft, we chose to use the perimeter to calculate the equivalent circle area instead of the luminal area of the graft. The proportion of collagen was also calculated by ImageJ (Version 1.52a).

## 2.10. Mechanical testing

According to previous study [38], for a hoop tensile measurement, the graft segments were loaded on two steel rods which were mounted in a mechanical test machine (Xiangjie, Shanghai, China). With a rate of 10 mm/min, the stress-strain curves and maximum tensile strength were recorded until segments failure. The resisting area was calculated and obtained the Young's modulus from the linear phase of each curve.

## 2.11. Mercury intrusion porosimetry

Mercury intrusion porosimetry was used to characterize pore size distribution and porosity based on previous studies (AutoPore IV 9500, USA) [39,40]. The max pressure was set to 33,000 psi. A histogram of pore size was reported.

## 2.12. Quantification of residual elastase

Elastase substrate V (Sigma-Aldrich, 324740) was used to quantify the residual elastase of vascular grafts [41,42]. The cleavage products of the substrate generate fluorescence with an intensity that is directly proportional to the residual activity of the enzyme. The soak solution of wash and unwashed elastase-treated dTEVGs were respectively obtained, and PBS was as negative control. After adding substrate and incubating for 15 min at room temperature, the fluorescence excitation at 380 nm and emission at 460 nm were detected.

## 2.13. DNA and RNA quantification

DNA extraction from vascular grafts before and after decellularization was performed using a mouse tail genomic DNA kit (Kangweishiji, CW2094). RNA extraction was used Trizol (Accurate Biology, AG21102). DNA and RNA concentration was quantified (Thermo scientific, Nanodrop 2000) and was normalized according to the tissue weight [34].

## 2.14. Glycosaminoglycans quantification

Glycosaminoglycans (GAGs) contents of grafts were quantified with 1,9-dimethyl-methylene blue according to the manufacturer's instructions (G&V S 19239.2) and were normalized based on the tissue dry

weight [38].

## 2.15. PCNA and TUNEL assay

PCNA (CST, 13110T, 1:100) and TUNEL (Abcam, ab66110) assay were performed followed the manufacturer's instructions.

## 2.16. Platelet adhesion

Analysis was performed as described previously [43]. Briefly, whole blood from healthy Sprague-Dawley rats was collected in a vacuum tube containing EDTA. Platelet-rich plasma (PRP) was prepared by centrifuging the blood at 1200 rpm. 1 ml of fresh PRP was placed in 12-well plates with samples and incubated at 37 °C for 2 h and then removed from the well. After rinsing three times with normal saline to remove loosely adherent platelets on the samples, the samples were fixed in 2.5 % glutaraldehyde at 37 °C for 1 h. After dehydrated, the number of platelets on the sample surfaces was determined under SEM from different fields.

## 2.17. Statistical analysis

All analysis were conducted using Prism 8 software (GraphPad Software, Inc., La Jolla, CA). Gaussian distribution was confirmed with the Shapiro-Wilk test prior to performing parametric analyses. Student's t-test and one-way ANOVA were performed to compare the difference between groups. For data not confirming Gaussian distribution, the Mann-Whitney test was performed. Two-way ANOVA was used when comparing the difference of inner diameters in AVG models. Data are represented as mean  $\pm$  standard deviations. Significant level  $p = 0.05$  was set for all the tests. \* $P < 0.05$ , \*\* $P < 0.01$ , \*\*\* $P < 0.001$ , \*\*\*\* $P < 0.0001$ .

## 3. Result

### 3.1. Elastase-treated decellularized tissue-engineered vascular graft fabrication and characterization

The preparation of the elastase-treated dTEVG was shown in Fig. 1A. Carotid arteries were obtained from rats, and cellular components were effectively removed using CHAPS, SDS, DNase I and RNase A. In contrast to native carotid arteries, the dTEVGs showed significant decrease of DNA and RNA content (Fig S2). Subsequently, elastase-treated dTEVGs were obtained after treatment with elastase. The effects of different elastase treatment duration on dTEVGs were evaluated (Fig. 1B). As the elastase treatment duration increased, the transparency of dTEVGs gradually increased. Histological features of dTEVGs treated with different elastase durations were evaluated using H&E, EVG and Masson's trichrome staining (Fig. 1C). H&E staining confirmed completely decellularization. The cracks of elastic fibers, stained red, were observed in the elastase-treated groups. EVG staining more clearly showed that elastic fibers had cracks in dTEVGs after elastase treatment, and more cracks appeared with the increase of treatment duration. Notably, after 45-min treatment, elastic fibers showed numerous severe cracks (Fig. 1C and D). To assess the deformation of the graft's cross section, the area of collagen fibers was evaluated using Masson's trichrome staining. Compared with the control group, only the 45-min elastase treatment significantly increased the collagen fiber area, indicating that the media structure of the dTEVG was deformed (Fig. 1C–E). The mechanical test was performed to evaluate the effect of elastase (Fig S3). Decellularization tended to decrease the maximum tensile force and Young's modulus of the grafts. Compared to normal carotid arteries, elastase treatment for 30 min resulted in a significant decrease in maximum tensile force, but no significant difference in Young's modulus. There was no significant difference between control and 30-min treated groups. Both maximum tensile force and Young's modulus were



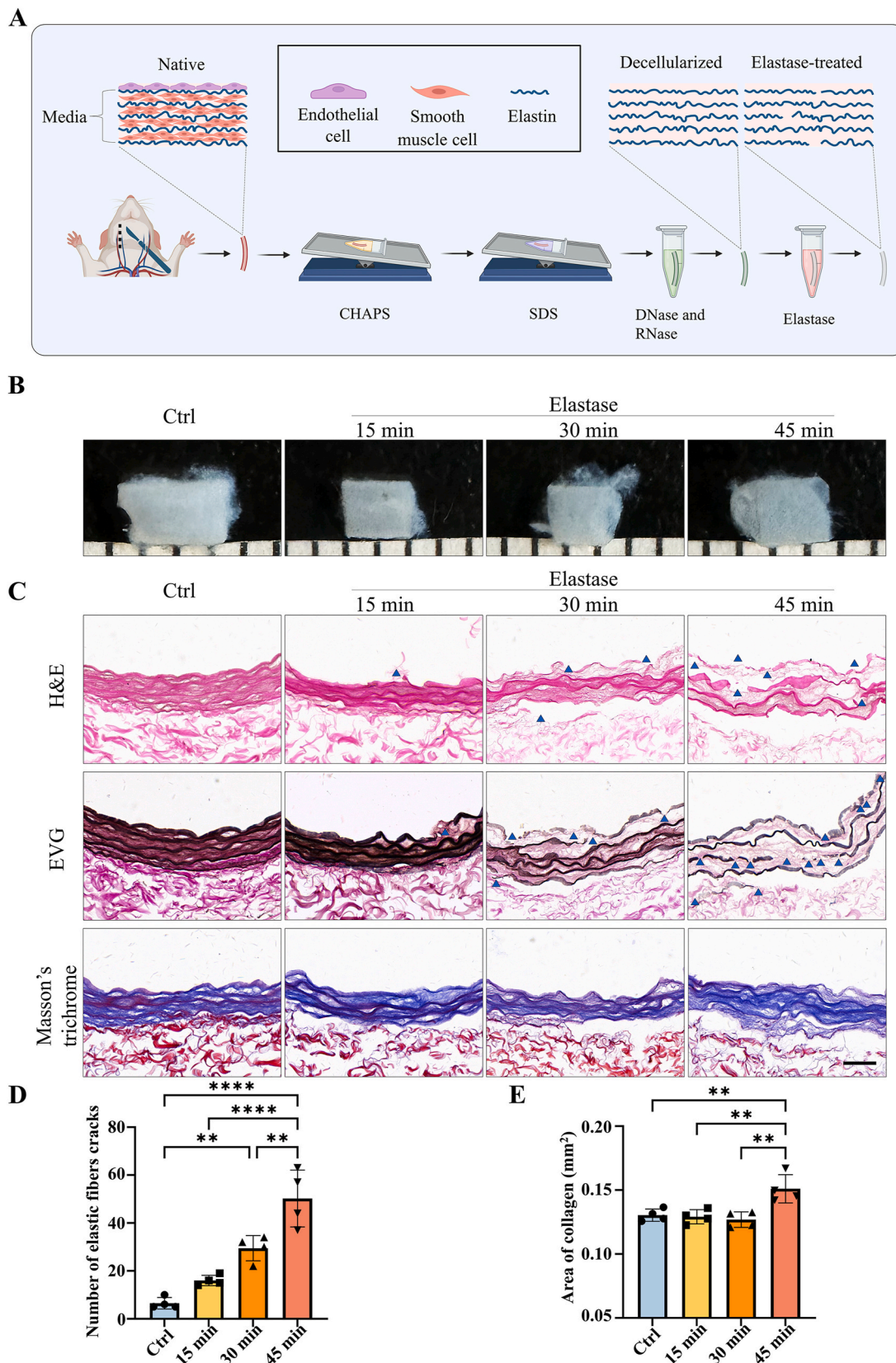


**Fig. 1. Elastase-treated decellularized tissue-engineered vascular graft fabrication and characterization.** A) Schematic illustrating the fabrication of the dTEVG. B) Image of dTEVGs with 0-, 15-, 30- and 45-min elastase treatment. C) H&E, EVG and Masson's trichrome staining of 0-, 15-, 30- and 45-min elastase-treated dTEVGs, the blue triangles marking the representative cracks (scale bar, 50  $\mu$ m). D) Number of elastic fiber cracks in elastase-treated dTEVGs with different treatment duration (n = 4, non-significant difference is not marked). E) Collagen area in cross sections of dTEVGs treated with elastase for different treatment duration (n = 4, non-significant difference is not marked). Data are represented as mean  $\pm$  standard deviations. \*P < 0.05, \*\*P < 0.01, \*\*\*P < 0.001, \*\*\*\*P < 0.0001.



significantly decreased after 45-min elastase treatment, suggesting its strong damaging effect on graft structure (Fig S3).

To further evaluate the difference between dTEVGs with or without elastase treatment, ultrastructure was analyzed using SEM (Fig. 2). Multiple positions of dTEVGs were depicted (Fig. 2A). SEM confirmed the efficient removal of cellular components (Fig. 2B). The abluminal surface of the dTEVG appeared dense, while it became loose after elastase treatment. The dTEVG exhibited a smooth and flat luminal surface. However, post-elastase treatment, the luminal surface became rough, with scattered holes and cracks observed in the elastic fiber layers (Fig. 2B). Compared with 15-min treatment, the 30-min treatment resulted in more numerous and pronounced holes on the luminal surface. However, after 45 min of treatment, the luminal surface of the dTEVG showed significant degradation and destruction, with extensive ruptures (Fig. 2B). These findings suggested that elastase treatment altered the dense structure, primarily causing scattered cracks and holes

in the elastic fiber layers of the dTEVGs.

### 3.2. Cell infiltration of elastase-treated decellularized tissue-engineered vascular grafts in subdermal implantation

To verify whether the cracks and holes in the elastic fiber layers caused by elastase treatment enhance the host cell infiltration, the dTEVGs were implanted subdermally in rats for 21 days. The structure of subdermally implanted dTEVGs was evaluated by H&E and EVG staining (Fig. 3A). Without elastase treatment, the dTEVG had complete and continuous elastic fibers, whereas after 15 and 30 min of elastase treatment, crack points appeared in the elastic fibers. However, after 45-min elastase treatment, the elastic fibers of the dTEVG showed severe degradation and structural fragmentation. DAPI staining was for assessing the cell infiltration (Fig. 3A). In the control group and 15-min elastase treatment group, only a few cells slightly infiltrated into the

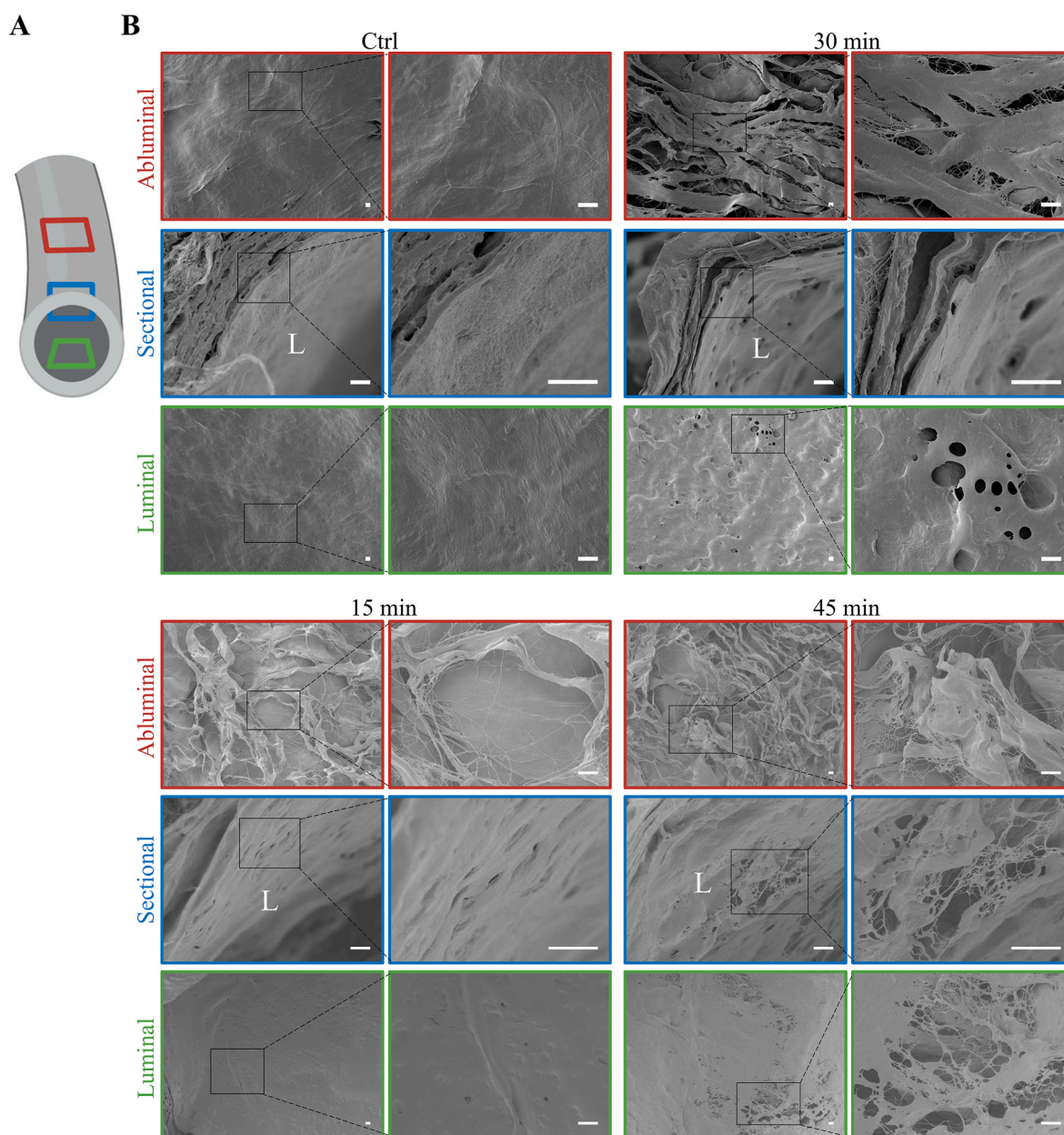


**Fig. 2.** Scanning electron microscopy assessment of ultrastructure of elastase-treated decellularized tissue-engineered vascular grafts. A) Schematic diagram of a dTEVG depicting sections taken for SEM. B) Comparison of ultrastructure among dTEVGs with 0-, 15-, 30-, 45-min elastase treatment (scale bar, 10  $\mu$ m). L: luminal.

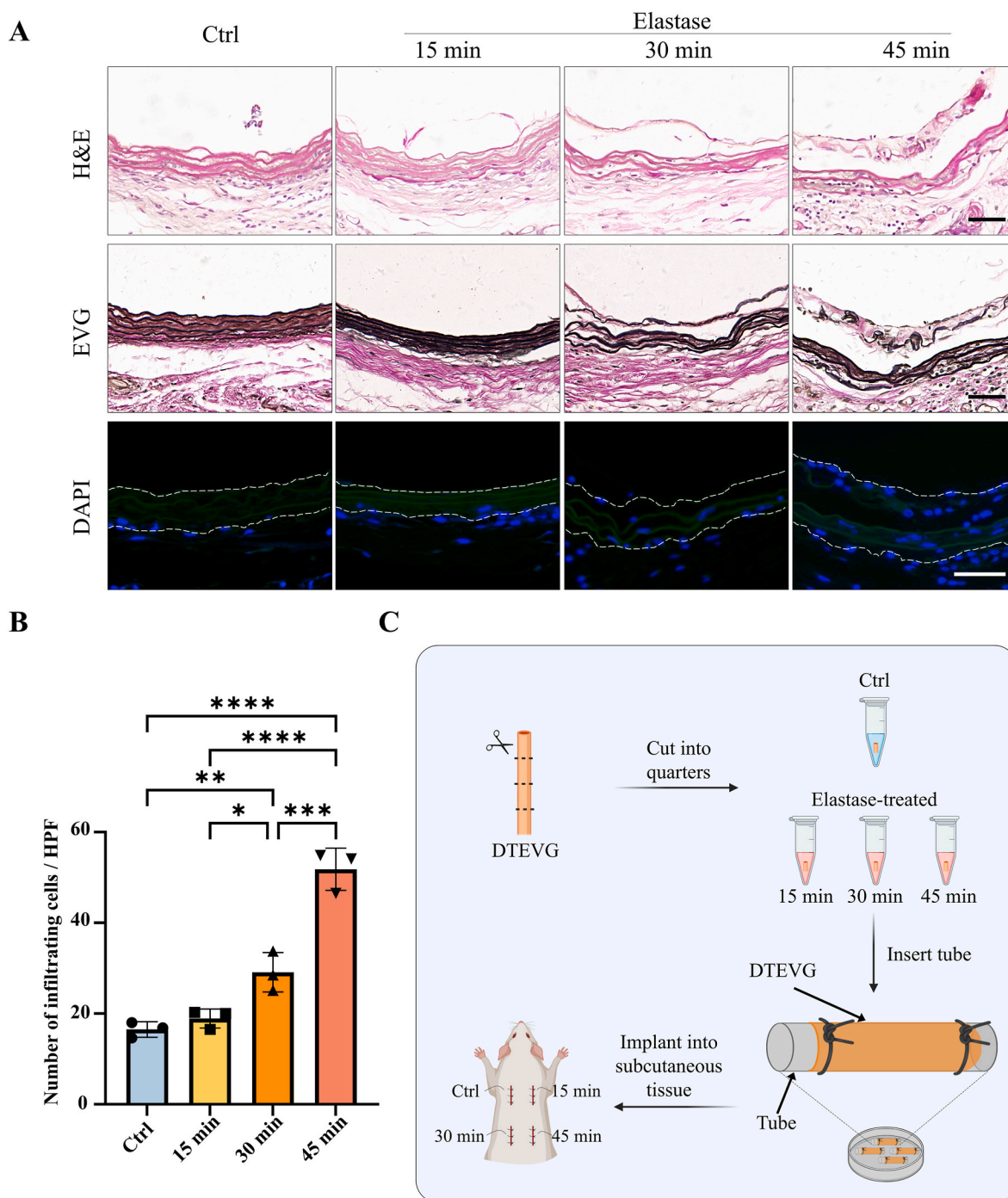


**Fig. 3. Subcutaneous implantation to evaluate cell infiltration in decellularized tissue-engineered vascular grafts with 0-, 15-, 30- and 45-min elastase treatment.** A) H&E, EVG and DAPI staining of 0-, 15-, 30- and 45-min elastase-treated dTEVGs, the dotted line showing the structure of the grafts (scale bar, 50  $\mu$ m). B) Number of cells infiltrating into the graft per high-power field in 0-, 15-, 30- and 45-min elastase-treated dTEVGs ( $n = 3$ , non-significant difference is not marked). C) Schematic illustrating the process of implantation control group and elastase-treated groups into the subcutaneous tissue of the rat. DTEVG: decellularized tissue-engineered vascular graft. Data are represented as mean  $\pm$  standard deviations. \* $P < 0.05$ , \*\* $P < 0.01$ , \*\*\* $P < 0.001$ , \*\*\*\* $P < 0.0001$ .

grafts, with most cells blocked outside the elastic fiber layer. However, 30 min of elastase treatment significantly promoted the infiltration and penetration of host cells in the dTEVG. In addition, 45-min elastase treatment further enhanced the infiltration of cells into the graft, with significant structural damage (Fig. 3A and B). Additionally, 30- and 45-min treatment significantly increase the number of infiltrating cells in both abluminal and luminal side of the grafts (Fig S4). The subdermal implantation process of the graft was shown in Fig. 3C. These results indicated that elastase treatment of dTEVGs for 30 min or more

enhanced the infiltration of cells.

### 3.3. Ultrasound and morphology of elastase-treated decellularized tissue-engineered vascular grafts in rat AVG models

According to above results, elastase treatment of the dTEVGs for 30 min significantly promoted the cell infiltration, with largely retaining the grafts' structure. In contrast, although 45-min treatment also enhanced cell infiltration, it led to obvious degradation and



destruction of the original structure of dTEVGs. Therefore, we chose a 30-min elastase treatment to achieve mild degradation and promote cell infiltration. After 30-min elastase treatment, the dTEVG had increased porosity and showed a higher distribution of pores in larger pore sizes

(Fig S5). The glycosaminoglycans (GAGs) content in normal carotid arteries was significantly reduced by decellularization process but not further by 30-min elastase treatment (Fig S6A). Furthermore, 30 min of treatment did not significantly alter platelet adhesion and morphology

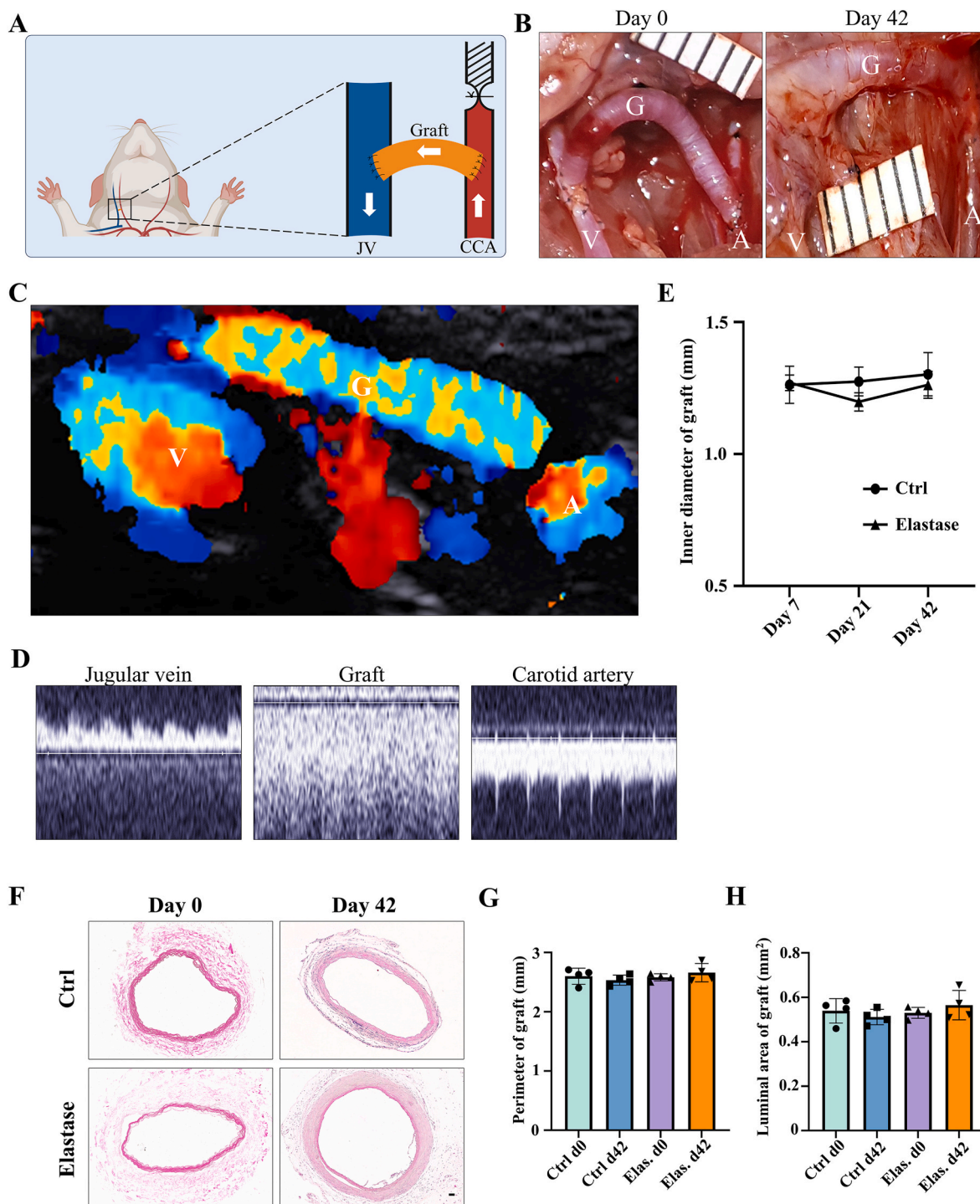


**Fig. 4.** Evaluation of ultrasound and morphology of mildly elastase-treated decellularized tissue-engineered vascular grafts in the rat arteriovenous graft models. A) Schematic illustrating the construction of the rat AVG models. B) The macroscopic morphology of mildly elastase-treated dTEVGs at day 0 and day 42. C) Color doppler blood flow imaging of mildly elastase-treated dTEVGs at day 42. D) Ultrasound spectral analysis of the carotid arteries, grafts and jugular veins in the rat AVG models. The appearance of AVG specific spectral patterns after transplantation indicating successful modeling. E) The inner diameters of mildly elastase-treated dTEVGs and control groups measured at day 7, 21 and 42 post-operations (n = 4, non-significant difference is not marked). F) Morphology of grafts assessed by H&E staining after decellularization, after mild elastase treatment, and after 42-day transplantation of both. G) Perimeter of grafts after decellularization, after mild elastase treatment, and after 42-day transplantation of both (n = 4, non-significant difference is not marked). H) Equivalent luminal area of grafts after decellularization, after mild elastase treatment, and after 42-day transplantation of both (n = 4, non-significant difference is not marked). Elas.: elastase treatment. V: vein. G: graft. A: artery. Data are represented as mean  $\pm$  standard deviations. \*P < 0.05, \*\*P < 0.01, \*\*\*P < 0.001, \*\*\*\*P < 0.0001.



(Fig S6B, C). 30-min elastase-treated dTEVGs were implanted into rats to create the AVGs between the carotid arteries and the jugular veins (Fig. 4A, Fig S7). There was no obvious blood oozing on the graft surface after transplantation. After 42 days, the graft was harvested, retaining its original shape, showing no sign of disintegration, and was covered with a thin capsule (Fig. 4B). Color doppler blood flow imaging and ultrasound spectrum analysis of the jugular vein, graft and carotid artery revealed that the mildly elastase-treated dTEVG remained patent and the AVG was constructed successfully (Fig. 4C and D). The inner

diameters calculated from the ultrasound test showed no significant stenosis or dilation and there was no significant difference compared to control group (Fig. 4E and Fig S8). H&E staining was used to further evaluate the morphological changes of grafts after elastase treatment or in vivo transplantation. After mild elastase treatment and 42 days of transplantation into the AVG models, the circumference and equivalent lumen area of grafts showed no significant change (Fig. 4F, G, H). These findings demonstrated that the dTEVGs, mildly treated with elastase, retained their morphology after transplantation for 42 days, without

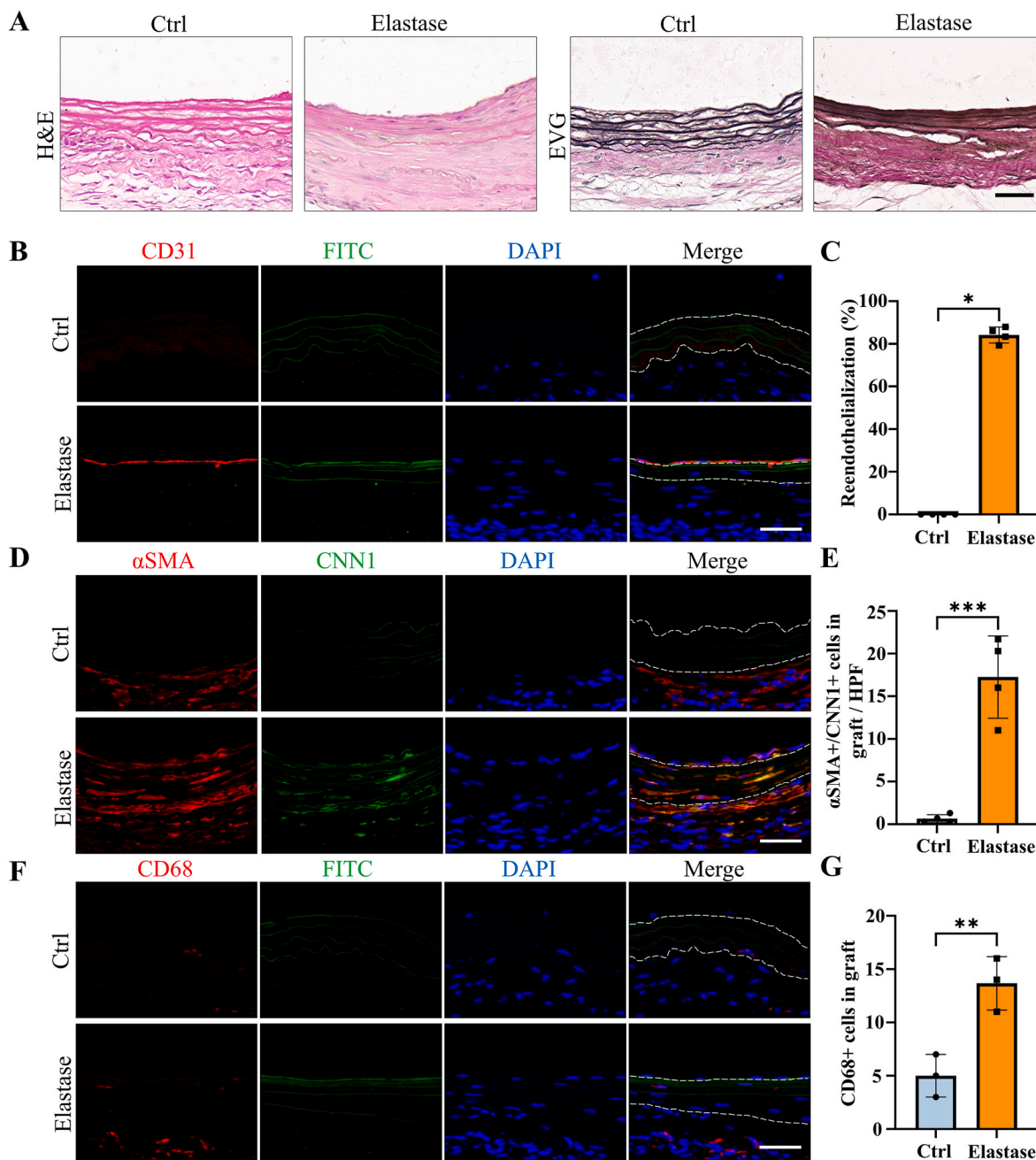


**Fig. 5.** Evaluation of cell infiltration and remodeling in mildly elastase-treated decellularized tissue-engineered vascular grafts in rat arteriovenous graft models. A) H&E and EVG staining of dTEVGs with or without mild elastase treatment after transplantation into rat AVG models for 42 days. B) Immunofluorescence staining of CD31 at day 42 between dTEVGs with or without mild elastase treatment. C) The proportion of reendothelialization in the whole lumen of dTEVGs with or without mild elastase treatment (n = 4). D) Immunofluorescence staining of  $\alpha$ -SMA and CNN1 at day 42 between dTEVGs with or without mild elastase treatment. E) The number of  $\alpha$ -SMA- and CNN1-positive cells in dTEVGs with or without mild elastase treatment (n = 4). F) Immunofluorescence staining of CD68 at day 42 between dTEVGs with or without mild elastase treatment. G) The number of CD68-positive cells in dTEVGs with or without mild elastase treatment (n = 3). The dotted line showing the structure of the grafts. Scale bar, 50  $\mu$ m. Data are represented as mean  $\pm$  standard deviations. \*P < 0.05, \*\*P < 0.01, \*\*\*P < 0.001, \*\*\*\*P < 0.0001.

obvious stenosis, dilation or disintegration.

### 3.4. Cell infiltration and remodeling of elastase-treated decellularized tissue-engineered vascular grafts in AVG models

H&E and EVG staining were employed to evaluate the structure and cell infiltration of dTEVGs. In the dTEVG, there was almost no cell infiltration in the graft, with most cells located outside the graft. In contrast, in the dTEVG mildly treated with elastase, cracks in elastic fibers were observed, and nucleated cells were homogeneously distributed between the elastic fibers (Fig. 5A). A layer of cells covered the lumen of the mildly elastase-treated dTEVG (Fig. 5A). To identify the types of infiltrating cells and the remodeling of the dTEVGs with or without elastase treatment, immunofluorescence was used. Given the importance of SMCs and ECs in natural blood vessels and dTEVGs, these two types were identified first. On day 42, the untreated dTEVG showed almost no nucleated cells or CD31-positive cells on the luminal side, indicating a lack of reendothelialization in the AVG. Nevertheless, the mildly elastase-treated dTEVG showed an impressive high degree of reendothelialization, with a continuous layer of ECs found on the lumen surface (Fig. 5B and C). In the 42-day AVG model,  $\alpha$ -SMA-positive cells were mainly distributed on the outside of the dTEVG, and only few infiltrated into the graft, but after mild elastase treatment, significantly more  $\alpha$ -SMA-positive cells infiltrated into the graft from the outside and homogeneously filled between the elastic fiber layers (Fig. 5D). In addition, we found that almost all of the  $\alpha$ -SMA-positive cells infiltrated in the graft was CNN1-positive, suggesting the regeneration of the mature contractile smooth muscle layers in the mildly elastase-treated dTEVG in the 42-day AVG rat model (Fig. 5D and E). Additionally, CD68-positive cells were also detected. Although both types of the grafts exhibited very few CD68-positive cells, the mildly elastase-treated dTEVG still had a higher number of CD68-positive cells (Fig. 5F and G).

### 3.5. Extracellular matrix secretion of elastase-treated decellularized tissue-engineered vascular grafts in AVG models

Extracellular matrix secretion plays a crucial role in the remodeling of vascular grafts. Therefore, collagen secretion was evaluated in dTEVGs with or without mild elastase treatment after 42-day transplantation in AVG models. Masson's trichrome staining revealed that, compared to the control group, the mildly elastase-treated dTEVG was filled with muscle fibers, demonstrating a densely infiltration of SMCs (Fig. 6A). Furthermore, the mildly elastase-treated dTEVG exhibited a higher proportion of collagen fibers at day 42, suggesting infiltrating cells involved in the synthesis of collagen fibers (Fig. 6B). We further investigated the distribution of young and mature collagen with Herovici's staining. The mature collagen was observed in the mildly elastase-treated dTEVG, but hardly in the control (Fig. 6C). Picrosirius red staining was utilized to identify collagen types in the grafts (Fig. 6D). Type I collagen, which was stained red or yellow, was found in the mildly elastase-treated dTEVG. Compared to the control group, the tissue surrounding the mildly elastase-treated dTEVG contained more proportion of type I collagen. Immunofluorescence further confirmed that type I and type III collagen proportions were increased in the mildly elastase-treated dTEVG, suggesting the remodeling of the graft (Fig. 6E and F).

## 4. Discussion

DTEVGs are natural blood vessels with cellular components removed and extracellular matrix components retained, which offers advantages such as good biocompatibility, low immunogenicity, and the potential to integrate with natural blood vessels [14–19]. However, the dense matrix structure of dTEVGs limits the cell infiltration and prevents remodeling [25,27,28,44]. It has been reported that  $\alpha$ -SMA-positive cell layers were not formed in the dTEVGs connecting the aorta and vena cava [24].

Another study showed the dTEVGs lacked sufficient remodeling with only patch-like aggregates of smooth muscle cells (SMCs) and partial luminal lining with endothelial cells (ECs) in the grafts after 14 weeks of transplantation [26]. Our previous results also demonstrated that the dTEVGs have unsatisfactory cell infiltration and remodeling in rat AVG models, especially in the middle segment of the grafts [33]. Various methods have been applied to increase the porosity of vascular grafts to improve cell infiltration [25,45]. Atsushi Mahara et al. fabricated pore structure in dTEVGs with femtosecond laser ablation and successfully improved the cell infiltration and graft regeneration [29]. Dong Yixiang et al. used short wave length ultraviolet radiation treatment to fabricate 3D scaffold with micropores and found SMCs migrate into the micropores [45]. Dan T. Simionescu et al. conducted a selective removal of vascular graft components to create porous grafts capable of facilitating cell infiltration [28]. But these in vivo experiments only involved subcutaneous implantation and did not replicate the circulatory system environment in which the grafts were used. Specifically, the subcutaneously implanted graft did not account for the influence of hemodynamics, ignoring the potential issues of dTEVGs, such as dilatation, aneurysmal degeneration and rupture [46,47]. Additionally, the subcutaneous implantation models lacked the effect of hemodynamics on the vascular cells [48]. Moreover, the subcutaneously implanted graft was infiltrated primarily by inflammatory cells, lacking interactions with important vascular cells, such as ECs and SMCs [29,49]. Consequently, these porous subcutaneously implanted grafts only increased the inflammation cell infiltration without achieving remodeling of SMCs or ECs, consistent with our results in subcutaneous implantation (Fig. S9). In contrast, improving the porosity of grafts have been shown to promote graft remodeling in the circulatory system environments, such as carotid artery replacement model and aorta replacement model, indicating that the different environments have important effects on the remodeling process [25,50]. It remains unknown that whether improving graft porosity will increase cell infiltration and interaction, then promote dTEVG remodeling in hemodialysis.

Given the dense components of dTEVGs mainly including elastic fibers and collagen fibers, we attempted to fabricating porous dTEVGs with elastase or collagenase. For the collagenase treatment we used, only a loosen abluminal surface was observed in the dTEVG, without obvious cracks or holes observed in the luminal surface. After transplantation into the rat AVG model for 42 days, there was no obviously increased cell infiltrating in that graft (Fig. S10). In contrast, the elastase treatment fabricated scattered cracks and holes in the elastic fiber layers of the dTEVG. We decided to increase the porosity of the dTEVG with elastase treatment to improve its cell infiltration and achieve its remodeling as the hemodialysis access. In order to preserve the original structure of the graft to cope with the complex environment in hemodialysis, such as withstanding the high speed of blood flow, we attempted to increase the porosity of elastic fiber layers rather than completely remove it. We evaluated the effects of three different duration of elastase treatment on the mechanical, macroscopic and histological changes of dTEVGs, and we assessed ultrastructural difference between the dTEVGs with or without elastase treatment with SEM. Finally, 30 min elastase treatment was determined to be a suitable mild treatment. The mildly elastase-treated dTEVGs were evaluated in vitro, subcutaneous implantation and rat AVG models. We found that: 1. Mild elastase-treated dTEVGs fabricated scattered cracks and holes in the elastic fiber layers, promoting cell infiltration with basically maintaining the structure; 2. Porous dTEVGs treated by mild elastase promoted cellular remodeling of smooth muscle layers and endothelium in the AVG models without stenosis, dilation or disintegration; 3. The remodeling of mildly elastase-treated dTEVGs had the ability of producing extracellular matrix.

SMCs are the main component of the media in native vessels which supports the structure, participates in the vasoactive response and involves in vascular remodeling [51]. SMCs can be roughly divided into contractile and synthetic phenotypes [52]. In native vessels, majority of

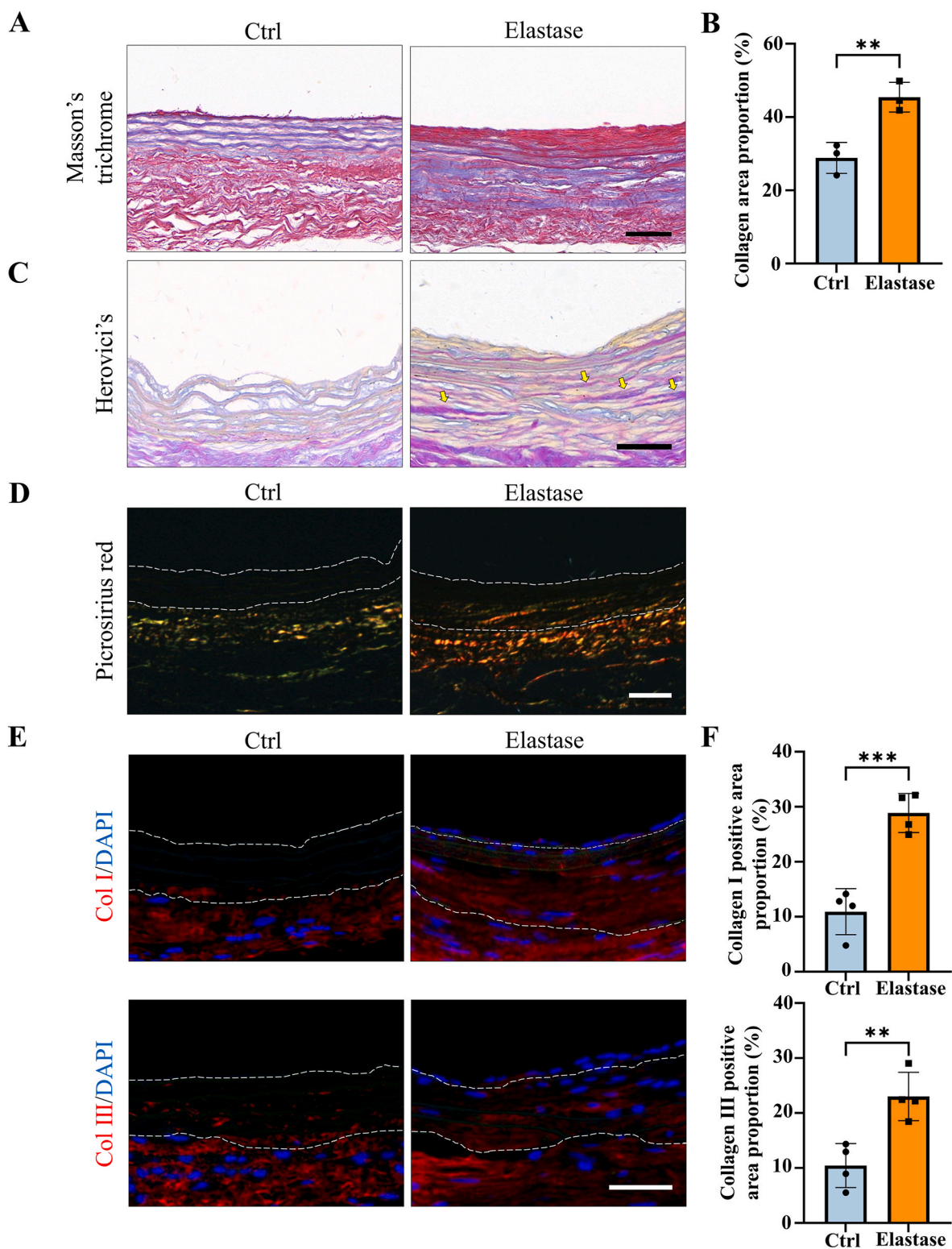


**Fig. 6. Evaluation of extracellular matrix remodeling in mildly elastase-treated decellularized tissue-engineered vascular grafts in the rat arteriovenous graft models.** A) Masson's trichrome staining of dTEVGs with or without mild elastase treatment at day 42 (scale bar, 50  $\mu$ m). B) The collagen area proportion of dTEVGs with or without mild elastase treatment at day 42 (n = 3). C) Herovici's staining of dTEVGs with or without mild elastase treatment at day 42, mature collagen indicated by yellow arrows (scale bar, 50  $\mu$ m). D) Picrosirius red staining of dTEVGs with or without mild elastase treatment at day 42 (scale bar, 50  $\mu$ m). E) The immunofluorescence staining of collagen I and III at day 42 between dTEVGs with or without mild elastase treatment (scale bar, 50  $\mu$ m). F) The positive area proportion of collagen I and III at day 42 in dTEVGs with or without mild elastase treatment (n = 4). The dotted line showing the structure of the grafts. Col I: collagen I. Col III: collagen III. Data are represented as mean  $\pm$  standard deviations. \*P < 0.05, \*\*P < 0.01, \*\*\*P < 0.001, \*\*\*\*P < 0.0001.



SMCs in media are contractile phenotypes, higher expression of contractile proteins such as  $\alpha$ -SMA, CNN and SMMHC, regulating vascular tone and diameter and blood pressure distribution through contraction and dilatation. Whereas, synthetic phenotypes have enhanced ability of proliferation, migration and secretion [53,54]. We used immunofluorescence to identify the phenotypes of SMCs infiltrating into our grafts. Our study indicated mild elastase treatment promoted  $\alpha$ -SMA-positive cells infiltrating into dTEVGs in rat AVG models, and almost all  $\alpha$ -SMA-positive cells in the graft were also CNN1-positive, suggesting the mildly elastase-treated dTEVGs have remodeled mature contractile smooth muscle layers [52,55–58]. Interestingly, we found that those SMCs outside the graft were CNN1-negative (Fig. 5D and Fig S11), suggesting that there was possible difference about the modulatory of contractile tone amplitude and maintenance between these two kinds of SMCs [59,60]. Additionally, compared with mildly elastase-treated dTEVGs, the dTEVGs without treatment appeared to contain more synthetic SMCs in peri-graft tissue (Fig S11). The infiltrating SMCs did not show obvious sign of proliferation and apoptosis (Fig S12). Many previous studies have shown that dTEVGs have failed infiltration of vascular SMCs, without organized SMC layer forming [24,26,33]. Without adequate SMC infiltration and functional smooth muscle layers formation, the dTEVG can't response to the physiologic contraction and dilatation [53]. More importantly, SMC ingrowth and new matrix deposition are essential for puncture healing in hemodialysis [61]. Our results showed that with mildly elastase treatment, the porous elastic fiber layers increased the infiltration of SMCs, and organized contractile smooth muscle layers formed in the dTEVGs, suggesting the potential of physiologic contraction and repair in hemodialysis.

Functional luminal endothelial cell layer prevents the triggering of the extrinsic blood coagulation pathway, senses and transduces hemodynamics into release of vasoactive molecules, and interacts with the SMCs to prevent graft neointimal hyperplasia [62–64]. Reendothelialization is critical for dTEVGs to avoid thrombosis and stenosis, and maintain long-term patency in hemodialysis [62,65,66]. Previous studies have reported the absence of complete and timely reendothelialization in dTEVGs and various methods have been attempted to achieve rapid and complete reendothelialization in grafts, such as surface modification with growth factors and cytokines, pre-seeded cell, hybrid-materials and bioreactor pretreatment [26,33,64]. Compared to these studies, we used a simple but effective method to improve reendothelialization. Our result showed that the mildly elastase-treated dTEVG achieved an impressive reendothelialization, nearly covering the entire lumen of the graft. Studies has shown the graft surface topography involved in the endothelial cell adhesion and alignment, and the roughness affected the adhesion and activity of ECs [67–69]. We observed a rough and porous surface of the dTEVG with the mild elastase treatment by SEM, which might be beneficial to the adhere of ECs. In addition, SMCs have various interaction with ECs and reendothelialization is associated with the underlying smooth muscle layer in graft remodeling [70]. Qunying Guo et al. has demonstrated Jagged1 expression in vascular SMCs promoted endothelial regeneration and functions in AVG remodeling [71]. Kazuya Miyagawa et al. found contact between SMCs and ECs drive the endothelial regeneration with BMPR2-mediated activation of Notch1 [72]. Jun Ren et al. found that SMCs supported endothelial regeneration through paracrine mechanism after artery injury [73]. Impressive reendothelialization might be attributed to the porous elastic fiber layers, adequate SMC infiltration and subsequent abundant interaction between SMCs and ECs in the mildly elastase-treated dTEVGs.

It has been reported that macrophage infiltration was the critical step during the vascular graft remodeling, so we detected CD68-positive cells in the dTEVGs [25,74]. Macrophages may stimulate cell migration into the grafts and regulate cell function and graft remodeling [25,75,76]. Macrophages synthesize and secrete growth factors and cytokines such as VEGF to regulate the endothelial cell proliferation [77]. It has been reported that the delicate balance of M1 and M2 phenotypes of

macrophages regulated the remodeling process of biomaterial grafts. Appropriate proinflammatory M1 phenotype at early stage and subsequent pro-regenerative M2 phenotype participate in the graft remodeling together [78]. In our study, we observed very few CD68-positive cells in the dTEVGs with or without mild elastase treatment, indicating that the inflammation had subsided and the grafts had tended to be stabilized at 42 days [33,78]. But the number of CD68-positive cells in mildly elastase-treated group at 42 days still were a little more than that in control group. Notably, some of these cells in mildly elastase-treated dTEVGs exhibited an anti-inflammatory M2 phenotype, suggesting a stronger inflammation and repair process (Fig S13).

In addition to cellular remodeling, we also found remodeling of extracellular matrix in the grafts. Our data demonstrated that the mildly elastase-treated dTEVG formed the mature collagen fibers and had higher proportion of collagen at the day 42, indicating that the infiltrated cells had the ability to synthesize their own collagen. Collagen involves in the circumferential load bearing, withstanding physiological pulsatile pressure and provide attachment and interaction for vascular cells [79,80]. Lack of the collagen network reduced the tensile strength of vascular grafts [31]. If synthesis of collagen is not substantial enough, the grafts will lose the mechanical strength, leading to aneurysms, rupture, and even death [25]. Especially when used as AVGs, the grafts must be subjected to frequent puncture with large-pore needles [81,82]. Effective cell infiltration and new extracellular matrix deposition can achieve improvement of mechanical strength, healing the needle punctures and timely hemostasis in dTEVGs, without the formation of pseudoaneurysm [61,83]. To further differentiate type I and type III collagen, picrosirius red and immunofluorescence staining were performed. Our results confirmed that the collagen, type I and type III, was regenerated in the mildly elastase-treated dTEVGs at 42 days. Type III collagen is crucial for vascular development and is the predominant subtype in the initial stage of remodeling, while type I collagen increases in the ending stage [84–87]. The impressively high proportion of type I demonstrated that the porous elastic fiber layers accelerated the remodeling and maturation process of the dTEVGs. Interestingly, based on the results of picrosirius red staining, the peripheral tissue of the elastase-treated dTEVG was dominated by type I collagen, while that of the untreated dTEVG contained more type III collagen. The incorporation of peri-graft tissue is important for vascular graft stabilizing. Poor incorporation may cause peri-graft seroma in AVGs [85,88]. The difference in collagen composition in the peri-graft tissues in our study may be associated with different incorporation state, requiring further exploration for its biological function and clinical significance. Additionally, excessive and aberrant extracellular matrix accumulation may lead to vessel wall fibrosis response, with stiffer and less compliant vessel walls, such as allograft vasculopathy and vein graft disease [89–91]. After the realization of recellularization and remodeling, precise regulation of extracellular matrix accumulation may be helpful for a longer use duration of vascular grafts. In brief, our results demonstrated that the porous elastic fiber layers in the mildly elastase-treated dTEVGs promoted and accelerated the graft remodeling, and the infiltrated cells in the grafts were able to form the collagen to maintain the strength of the grafts and had the potential to repair the puncture.

## 5. Conclusion

This study demonstrates that elastase treatment induces scattered cracks and holes in the elastic fiber layers. The improved porosity of mildly elastase-treated dTEVGs promotes graft remodeling, involving smooth muscle layer formation, reendothelialization and extracellular matrix repair, restoring the biological function while retaining a stable structure. These improvements should aid in the better design of the next generation of vascular grafts for durable hemodialysis access.

## CRediT authorship contribution statement

**Tun Wang:** Writing – review & editing, Methodology, Funding acquisition, Conceptualization. **Sheng Liao:** Writing – original draft, Methodology, Investigation, Formal analysis. **Peng Lu:** Methodology, Investigation. **Zhenyu He:** Methodology. **Siyuan Cheng:** Methodology. **Tianjian Wang:** Investigation. **Zibo Cheng:** Methodology. **Yangyang An:** Methodology. **Mo Wang:** Methodology. **Chang Shu:** Supervision, Funding acquisition, Conceptualization.

## Declaration of competing interest

The authors declare that they have no known competing financial interests or personal relationships that could have appeared to influence the work reported in this paper.

## Acknowledgements

This work is financially supported by projects of International Cooperation and Exchanges National Natural Science Foundation of China (82120108005), National Natural Science Foundation of China (81900695) and Natural Science Foundation of Hunan Province of China (2021JJ40874, 2024JJ5466).

## Appendix A Supplementary data

Supplementary data to this article can be found online at <https://doi.org/10.1016/j.mtbio.2024.101402>.

## Abbreviations

dTEVG	decellularized tissue-engineered vascular graft
AVG	arteriovenous graft
SMC	smooth muscle cell
CKD	chronic kidney disease
ESRD	end-stage renal disease
ePTFE	expanded polytetrafluoroethylene
EC	endothelial cell
CA	carotid artery
SD	Sprague-Dawley
SEM	scanning electron microscope
H&E	Hematoxylin and eosin
EVG	Elastica Van Gieson
IACUC	Institutional Animal Care and Use Committee

## Data availability

Data will be made available on request.

## References

- M. Ruiz-Ortega, S. Rayego-Mateos, S. Lamas, A. Ortiz, R.R. Rodrigues-Diez, Targeting the progression of chronic kidney disease, *Nat. Rev. Nephrol.* 16 (5) (2020) 269–288, <https://doi.org/10.1038/s41581-019-0248-y>.
- K. Kalantar-Zadeh, T.H. Jafar, D. Nitsch, B.L. Neuen, V. Perkovic, Chronic kidney disease, *Lancet* 398 (10302) (2021) 786–802, [https://doi.org/10.1016/s0140-6736\(21\)00519-5](https://doi.org/10.1016/s0140-6736(21)00519-5).
- V. Jha, G. Garcia-Garcia, K. Iseki, Z. Li, S. Naicker, B. Plattner, R. Saran, A.Y. Wang, C.W. Yang, Chronic kidney disease: global dimension and perspectives, *Lancet* 382 (9888) (2013) 260–272, [https://doi.org/10.1016/s0140-6736\(13\)60687-x](https://doi.org/10.1016/s0140-6736(13)60687-x).
- Global, regional, and national burden of chronic kidney disease, 1990–2017: a systematic analysis for the Global Burden of Disease Study 2017, *Lancet* 395 (10225) (2020) 709–733, [https://doi.org/10.1016/s0140-6736\(20\)30045-3](https://doi.org/10.1016/s0140-6736(20)30045-3).
- T. Liyanage, T. Ninomiya, V. Jha, B. Neal, H.M. Patrice, I. Okpechi, M.H. Zhao, J. Lv, A.X. Garg, J. Knight, A. Rodgers, M. Gallagher, S. Kotwal, A. Cass, V. Perkovic, Worldwide access to treatment for end-stage kidney disease: a systematic review, *Lancet* 385 (9981) (2015) 1975–1982, [https://doi.org/10.1016/s0140-6736\(14\)61601-9](https://doi.org/10.1016/s0140-6736(14)61601-9).
- T.J. Vachharajani, J.J. Taliencio, E. Anvari, New devices and technologies for hemodialysis vascular access: a review, *Am. J. Kidney Dis.* 78 (1) (2021) 116–124, <https://doi.org/10.1053/j.ajkd.2020.11.027>.
- P. Sawo, A. Moufarrej, M. Sloff, M.G. Snoeijfs, T. Delhaas, J.H.M. Tordoir, B.M. E. Mees, The effect of geometric graft modification on arteriovenous graft patency in haemodialysis patients: a systematic review and meta-analysis, *Eur. J. Vasc. Endovasc. Surg.* 60 (4) (2020) 568–577, <https://doi.org/10.1016/j.ejvs.2020.06.023>.
- C.E. Lok, T.S. Huber, T. Lee, S. Shenoy, A.S. Yevzlin, K. Abreo, M. Allon, A. Asif, B. C. Astor, M.H. Glickman, J. Graham, L.M. Moist, D.K. Rajan, C. Roberts, T. J. Vachharajani, R.P. Valentini, KDOQI clinical practice guideline for vascular access: 2019 update, *Am. J. Kidney Dis.* 75 (4 Suppl 2) (2020) S1–S164, <https://doi.org/10.1053/j.ajkd.2019.12.001>.
- L.J. Arhuidese, M.A. Cooper, M. Rizwan, B. Nejim, M.B. Malas, Vascular access for hemodialysis in the elderly, *J. Vasc. Surg.* 69 (2) (2019) 517–525.e1, <https://doi.org/10.1016/j.jvs.2018.05.219>.
- R.K. Hall, E.R. Myers, S.E. Rosas, A.M. O'Hare, C.S. Colón-Emeric, Choice of hemodialysis access in older adults: a cost-effectiveness analysis, *Clin. J. Am. Soc. Nephrol.* 12 (6) (2017) 947–954, <https://doi.org/10.2215/cjn.11631116>.
- R. Dukkipati, M. Peck, R. Dharmija, D.M. Hentschel, T. Reynolds, G. Tammewar, T. McAllister, Biological grafts for hemodialysis access: historical lessons, state-of-the-art and future directions, *Semin. Dial.* 26 (2) (2013) 233–239, <https://doi.org/10.1111/j.1525-139X.2012.01106.x>.
- R.J. Manson, J.M. Unger, A. Ali, S.M. Gage, J.H. Lawson, Tissue-engineered vascular grafts: autologous off-the-shelf vascular access? *Semin. Nephrol.* 32 (6) (2012) 582–591, <https://doi.org/10.1016/j.semnephrol.2012.10.010>.
- J.M. Delorme, R. Guidoin, S. Canizales, J. Charara, T. How, Y. Marois, M. Batt, P. Hallade, M. Ricci, C. Picetti, et al., Vascular access for hemodialysis: pathologic features of surgically excised ePTFE grafts, *Ann. Vasc. Surg.* 6 (6) (1992) 517–524, <https://doi.org/10.1007/bf02000823>.
- D.G. Seifu, A. Purnama, K. Mequanint, D. Mantovani, Small-diameter vascular tissue engineering, *Nat. Rev. Cardiol.* 10 (7) (2013) 410–421, <https://doi.org/10.1038/nrcardio.2013.77>.
- S.L. Dahl, A.P. Kypson, J.H. Lawson, J.L. Blum, J.T. Strader, Y. Li, R.J. Manson, W. E. Tente, L. DiBernardo, M.T. Hensley, R. Carter, T.P. Williams, H.L. Prichard, M. S. Dey, K.G. Begelman, L.E. Niklason, Readily available tissue-engineered vascular grafts, *Sci. Transl. Med.* 3 (68) (2011) 68ra9, <https://doi.org/10.1126/scitranslmed.3001426>.
- K. Österberg, Y. Bogestål, L. Jenndahl, T. Gustafsson-Hedberg, J. Synnergren, G. Holmgren, E. Bom, S. Petronis, A. Krona, J.S. Eriksson, J. Rosendahl, V. Crisostomo, F.M. Sanchez-Margallo, C. Baez-Diaz, R. Strehl, J. Håkansson, Personalized tissue-engineered veins - long term safety, functionality and cellular transcriptome analysis in large animals, *Biomater. Sci.* 11 (11) (2023) 3860–3877, <https://doi.org/10.1039/d2bm02011d>.
- X. Wang, V. Chan, P.R. Corridon, Decellularized blood vessel development: current state-of-the-art and future directions, *Front. Bioeng. Biotechnol.* 10 (2022) 951644, <https://doi.org/10.3389/fbioe.2022.951644>.
- D. Choudhury, M. Yee, Z.L.J. Sheng, A. Amirul, M.W. Naing, Decellularization systems and devices: state-of-the-art, *Acta Biomater.* 115 (2020) 51–59, <https://doi.org/10.1016/j.actbio.2020.07.060>.
- Q. Cai, W. Liao, F. Xue, X. Wang, W. Zhou, Y. Li, W. Zeng, Selection of different endothelialization modes and different seed cells for tissue-engineered vascular graft, *Bioact. Mater.* 6 (8) (2021) 2557–2568, <https://doi.org/10.1016/j.bioactmat.2020.12.021>.
- B. Weber, M.Y. Emmert, R. Schoenauer, C. Brokopp, L. Baumgartner, S. P. Hoerstrup, Tissue engineering on matrix: future of autologous tissue replacement, *Semin. Immunopathol.* 33 (3) (2011) 307–315, <https://doi.org/10.1007/s00281-011-0258-8>.
- I. Arhuidese, T. Reifsnnyder, T. Islam, O. Karim, B. Nejim, T. Obeid, U. Qazi, M. Malas, Bovine carotid artery biologic graft outperforms expanded polytetrafluoroethylene for hemodialysis access, *J. Vasc. Surg.* 65 (3) (2017) 775–782, <https://doi.org/10.1016/j.jvs.2016.10.080>.
- D.M. Pineda, M.J. Dougherty, M.C. Wismer, C. Carroll, S. Tyagi, D.A. Troutman, K. D. Calligaro, Bovine carotid artery xenografts for hemodialysis access, *J. Vasc. Surg.* 65 (6) (2017) 1729–1734, <https://doi.org/10.1016/j.jvs.2016.12.109>.
- C.R. Darby, D. Roy, D. Deardon, A. Cornall, Depopulated bovine ureteric xenograft for complex haemodialysis vascular access, *Eur. J. Vasc. Endovasc. Surg.* 31 (2) (2006) 181–186, <https://doi.org/10.1016/j.ejvs.2005.07.006>.
- H. Bai, A. Dardik, Y. Xing, Decellularized carotid artery functions as an arteriovenous graft, *J. Surg. Res.* 234 (2019) 33–39, <https://doi.org/10.1016/j.jss.2018.08.008>.
- Z. Wang, Y. Cui, J. Wang, X. Yang, Y. Wu, K. Wang, X. Gao, D. Li, Y. Li, X.L. Zheng, Y. Zhu, D. Kong, Q. Zhao, The effect of thick fibers and large pores of electrospun poly( $\epsilon$ -caprolactone) vascular grafts on macrophage polarization and arterial regeneration, *Biomaterials* 35 (22) (2014) 5700–5710, <https://doi.org/10.1016/j.biomaterials.2014.03.078>.
- U. Böer, C. Spengler, D. Jonigk, M. Klingenberg, C. Schrimpf, S. Litzner, M. Harder, H.H. Kreipe, A. Haverich, M. Wilhelm, Coating decellularized equine carotid arteries with CCN1 improves cellular repopulation, local biocompatibility, and immune response in sheep, *Tissue Eng Part A* 19 (15–16) (2013) 1829–1842, <https://doi.org/10.1089/ten.TEA.2012.0558>.
- J. Negishi, Y. Hashimoto, A. Yamashita, T. Kimura, A. Kishida, S. Funamoto, Histological structure affects recellularization of decellularized arteries, *Mater Sci Eng C Mater Biol Appl* 70 (Pt 1) (2017) 450–455, <https://doi.org/10.1016/j.msec.2016.09.004>.

- [28] D.T. Simionescu, Q. Lu, Y. Song, J.S. Lee, T.N. Rosenbalm, C. Kelley, N. R. Vyavahare, Biocompatibility and remodeling potential of pure arterial elastin and collagen scaffolds, *Biomaterials* 27 (5) (2006) 702–713, <https://doi.org/10.1016/j.biomaterials.2005.06.013>.
- [29] A. Mahara, K. Kojima, M. Yamamoto, Y. Hirano, T. Yamaoka, Accelerated tissue regeneration in decellularized vascular grafts with a patterned pore structure, *J. Mater. Chem. B* 10 (14) (2022) 2544–2550, <https://doi.org/10.1039/d1tb02271g>.
- [30] J. Cheng, J. Li, Z. Cai, Y. Xing, C. Wang, L. Guo, Y. Gu, Decellularization of porcine carotid arteries using low-concentration sodium dodecyl sulfate, *Int. J. Artif. Organs* 44 (7) (2021) 497–508, <https://doi.org/10.1177/0391398820975420>.
- [31] Q. Lu, K. Ganesan, D.T. Simionescu, N.R. Vyavahare, Novel porous aortic elastin and collagen scaffolds for tissue engineering, *Biomaterials* 25 (22) (2004) 5227–5237, <https://doi.org/10.1016/j.biomaterials.2003.12.019>.
- [32] T. Eufrazio-da-Silva, E. Ruiz-Hernandez, J. O'Dwyer, D. Picazo-Frutos, G.P. Duffy, B.P. Murphy, Enhancing medial layer recellularization of tissue-engineered blood vessels using radial microchannels, *Regen. Med.* 14 (11) (2019) 1013–1028, <https://doi.org/10.2217/rme-2019-0011>.
- [33] T. Wang, P. Lu, Z. Wan, Z. He, S. Cheng, Y. Zhou, S. Liao, M. Wang, T. Wang, C. Shu, Adaptation process of decellularized vascular grafts as hemodialysis access in vivo, *Regen Biomater* 11 (2024), <https://doi.org/10.1093/rb/rbae029>.
- [34] H. Bai, P. Sun, H. Wu, S. Wei, B. Xie, W. Wang, Y. Hou, J. Li, A. Dardik, Z. Li, The application of tissue-engineered fish swim bladder vascular graft, *Commun. Biol.* 4 (1) (2021) 1153, <https://doi.org/10.1038/s42003-021-02696-9>.
- [35] B. Jiang, B. Akgun, R.C. Lam, G.A. Ameer, J.A. Wertheim, A polymer-extracellular matrix composite with improved thromboresistance and recellularization properties, *Acta Biomater.* 18 (2015) 50–58, <https://doi.org/10.1016/j.actbio.2015.02.015>.
- [36] J. Liu, B. Li, H. Jing, Y. Wu, D. Kong, X. Leng, Z. Wang, Swim bladder as a novel biomaterial for cardiovascular materials with anti-calcification properties, *Adv Health Mater* 9 (2) (2020) e1901154, <https://doi.org/10.1002/adhm.201901154>.
- [37] A. Mahara, M. Kitai, H. Masunaga, T. Hikima, Y. Ohya, S. Sasaki, S. Sakurai, T. Yamaoka, Modification of decellularized vascular xenografts with 8-arm polyethylene glycol suppresses macrophage infiltration but maintains graft degradability, *J. Biomed. Mater. Res.* 108 (10) (2020) 2005–2014, <https://doi.org/10.1002/jbm.a.36960>.
- [38] K.H. Schneider, P. Aigner, W. Holthöner, X. Monforte, S. Nürnberger, D. Rünzler, H. Redl, A.H. Teuschl, Decellularized human placenta chorion matrix as a favorable source of small-diameter vascular grafts, *Acta Biomater.* 29 (2016) 125–134, <https://doi.org/10.1016/j.actbio.2015.09.038>.
- [39] J. Cheng, C. Wang, Y. Gu, Combination of freeze-thaw with detergents: a promising approach to the decellularization of porcine carotid arteries, *Bio Med. Mater. Eng.* 30 (2) (2019) 191–205, <https://doi.org/10.3233/bme-191044>.
- [40] M. Rodriguez, J.A. Kluge, D. Smoot, M.A. Kluge, D.F. Schmidt, C.R. Paetsch, P. S. Kim, D.L. Kaplan, Fabricating mechanically improved silk-based vascular grafts by solution control of the gel-spinning process, *Biomaterials* 230 (2020) 119567, <https://doi.org/10.1016/j.biomaterials.2019.119567>.
- [41] K. Nakajima, J.C. Powers, B.M. Ashe, M. Zimmerman, Mapping the extended substrate binding site of cathepsin G and human leukocyte elastase. Studies with peptide substrates related to the alpha 1-protease inhibitor reactive site, *J. Biol. Chem.* 254 (10) (1979) 4027–4032.
- [42] T. Alsaigh, E.S. Pocock, J.J. Bergan, G.W. Schmid-Schönbein, Acute venous occlusion enhances matrix metalloproteinase activity: implications on endothelial dysfunction, *Microvasc. Res.* 81 (1) (2011) 108–116, <https://doi.org/10.1016/j.mvr.2010.09.010>.
- [43] S. Liu, C. Dong, G. Lu, Q. Lu, Z. Li, D.L. Kaplan, H. Zhu, Bilayered vascular grafts based on silk proteins, *Acta Biomater.* 9 (11) (2013) 8991–9003, <https://doi.org/10.1016/j.actbio.2013.06.045>.
- [44] O.E. Teebken, A. Bader, G. Steinhoff, A. Haverich, Tissue engineering of vascular grafts: human cell seeding of decellularised porcine matrix, *Eur. J. Vasc. Endovasc. Surg.* 19 (4) (2000) 381–386, <https://doi.org/10.1053/ejvs.1999.1004>.
- [45] D. Yixiang, T. Yong, S. Liao, C.K. Chan, S. Ramakrishna, Degradation of electrospun nanofiber scaffold by short wave length ultraviolet radiation treatment and its potential applications in tissue engineering, *Tissue Eng Part A* 14 (8) (2008) 1321–1329, <https://doi.org/10.1089/ten.tea.2007.0395>.
- [46] R. Coscas, S. Dupont, S. Mussot, L. Louedec, H. Etienne, M. Morvan, G. Chiochia, Z. Massy, M.P. Jacob, J.B. Michel, Exploring antibody-dependent adaptive immunity against aortic extracellular matrix components in experimental aortic aneurysms, *J. Vasc. Surg.* 68 (6s) (2018) 60S–71S.e3, <https://doi.org/10.1016/j.jvs.2017.11.090>.
- [47] A.M. Ostidiek, J.R. Ivey, D.A. Grant, J. Gopaldas, S.A. Grant, An in vivo study of a gold nanocomposite biomaterial for vascular repair, *Biomaterials* 65 (2015) 175–183, <https://doi.org/10.1016/j.biomaterials.2015.06.045>.
- [48] S. Liu, Z. Lin, Vascular smooth muscle cells mechanosensitive regulators and vascular remodeling, *J. Vasc. Res.* 59 (2) (2022) 90–113, <https://doi.org/10.1159/000519845>.
- [49] Y. Liu, C. Chen, X. Xie, H. Yuan, Z. Tang, T. Qian, Y. Liu, M. Song, S. Liu, T. Lu, Z. Wu, Photooxidation and pentagalloyl glucose cross-linking improves the performance of decellularized small-diameter vascular xenograft in vivo, *Front. Bioeng. Biotechnol.* 10 (2022) 816513, <https://doi.org/10.3389/fbioe.2022.816513>.
- [50] J. Liu, Y. Qin, Y. Wu, Z. Sun, B. Li, H. Jing, C. Zhang, C. Li, X. Leng, Z. Wang, D. Kong, The surrounding tissue contributes to smooth muscle cells' regeneration and vascularization of small diameter vascular grafts, *Biomater. Sci.* 7 (3) (2019) 914–925, <https://doi.org/10.1039/c8bm01277f>.
- [51] R. Chakraborty, F.Z. Saddouk, A.C. Carrao, D.S. Krause, D.M. Greif, K.A. Martin, Promoters to study vascular smooth muscle, *Arterioscler. Thromb. Vasc. Biol.* 39 (4) (2019) 603–612, <https://doi.org/10.1161/atvbaha.119.312449>.
- [52] M. Liu, D. Gomez, Smooth muscle cell phenotypic diversity, *Arterioscler. Thromb. Vasc. Biol.* 39 (9) (2019) 1715–1723, <https://doi.org/10.1161/atvbaha.119.312131>.
- [53] P. Petsophonsakul, M. Furmanik, R. Forsythe, M. Dweck, G.W. Schurink, E. Natour, C. Reutelingsperger, M. Jacobs, B. Mees, L. Schurgers, Role of vascular smooth muscle cell phenotypic switching and calcification in aortic aneurysm formation, *Arterioscler. Thromb. Vasc. Biol.* 39 (7) (2019) 1351–1368, <https://doi.org/10.1161/atvbaha.119.312787>.
- [54] G. Cao, X. Xuan, J. Hu, R. Zhang, H. Jin, H. Dong, How vascular smooth muscle cell phenotype switching contributes to vascular disease, *Cell Commun. Signal.* 20 (1) (2022) 180, <https://doi.org/10.1186/s12964-022-00993-2>.
- [55] M. Furmanik, M. Chatrou, R. van Gorp, A. Akbulut, B. Willems, H. Schmidt, G. van Eys, M.L. Bochaton-Piallat, D. Proudfoot, E. Biessen, U. Hedin, L. Perisic, B. Mees, C. Shanahan, C. Reutelingsperger, L. Schurgers, Reactive oxygen-forming Nox5 links vascular smooth muscle cell phenotypic switching and extracellular vesicle-mediated vascular calcification, *Circ. Res.* 127 (7) (2020) 911–927, <https://doi.org/10.1161/circresaha.119.316159>.
- [56] L. Bianchi, I. Damiani, S. Castiglioni, A. Carleo, R. De Salvo, C. Rossi, A. Corsini, S. Bellosta, Smooth muscle cell phenotypic switch induced by traditional cigarette smoke condensate: a holistic overview, *Int. J. Mol. Sci.* 24 (7) (2023), <https://doi.org/10.3390/ijms24076431>.
- [57] C. Knox, K. Garcia, J. Tran, S.M. Wilson, A.B. Blood, M. Kearns-Jonker, T. P. Martens, A biomimetic approach utilizing pulsatile perfusion generates contractile vascular grafts, *Tissue Eng Part A* 29 (13–14) (2023) 358–371, <https://doi.org/10.1089/ten.TEA.2022.0206>.
- [58] D. Tiemessen, P. de Jonge, W. Daamen, W. Feitz, P. Geutjes, E. Oosterwijk, The effect of a cyclic uniaxial strain on urinary bladder cells, *World J. Urol.* 35 (10) (2017) 1531–1539, <https://doi.org/10.1007/s00345-017-2013-9>.
- [59] L.P. Kajuluri, Q.R. Lyu, J. Doja, A. Kumar, M.P. Wilson, S.R. Sgrizzi, E. Rezaeimanesh, J.M. Miano, K.G. Morgan, Calponin 1 inhibits agonist-induced ERK activation and decreases calcium sensitization in vascular smooth muscle, *J. Cell Mol. Med.* 28 (1) (2024) e18025, <https://doi.org/10.1111/jcmm.18025>.
- [60] R. Liu, J.P. Jin, Calponin isoforms CNN1, CNN2 and CNN3: regulators for actin cytoskeleton functions in smooth muscle and non-muscle cells, *Gene* 585 (1) (2016) 143–153, <https://doi.org/10.1016/j.gene.2016.02.040>.
- [61] B.W. Tillman, S.K. Yazdani, L.P. Neff, M.A. Corriere, G.J. Christ, S. Soker, A. Atala, R.L. Geary, J.J. Yoo, Bioengineered vascular access maintains structural integrity in response to arteriovenous flow and repeated needle puncture, *J. Vasc. Surg.* 56 (3) (2012) 783–793, <https://doi.org/10.1016/j.jvs.2012.02.030>.
- [62] J.W. Heng, M.D. Yazid, M.R. Abdul Rahman, N. Sulaiman, Coatings in decellularized vascular scaffolds for the establishment of a functional endothelium: a scoping review of vascular graft refinement, *Front Cardiovasc Med* 8 (2021) 677588, <https://doi.org/10.3389/fcvm.2021.677588>.
- [63] N. Dahan, U. Sarig, T. Bronshtein, L. Baruch, T. Karram, A. Hoffman, M. Machluf, Dynamic autologous reendothelialization of small-caliber arterial extracellular matrix: a preclinical large animal study, *Tissue Eng Part A* 23 (1–2) (2017) 69–79, <https://doi.org/10.1089/ten.TEA.2016.0126>.
- [64] H. Ding, X. Hou, Z. Gao, Y. Guo, B. Liao, J. Wan, Challenges and strategies for endothelializing decellularized small-diameter tissue-engineered vessel grafts, *Adv Health Mater* 13 (16) (2024) e2304432, <https://doi.org/10.1002/adhm.202304432>.
- [65] P. Zhao, Q. Fang, D. Gao, Q. Wang, Y. Cheng, Q. Ao, X. Wang, X. Tian, Y. Zhang, H. Tong, N. Yan, X. Hu, J. Fan, Klotho functionalization on vascular graft for improved patency and endothelialization, *Biomater. Adv.* 133 (2022) 112630, <https://doi.org/10.1016/j.msec.2021.112630>.
- [66] M.A.A. Fahad, H.Y. Lee, S. Park, M. Choi, P.C. Shanto, M. Park, S.H. Bae, B.T. Lee, Small-diameter vascular graft composing of core-shell structured micro-nanofibers loaded with heparin and VEGF for endothelialization and prevention of neointimal hyperplasia, *Biomaterials* 306 (2024) 122507, <https://doi.org/10.1016/j.biomaterials.2024.122507>.
- [67] S. Jana, Endothelialization of cardiovascular devices, *Acta Biomater.* 99 (2019) 53–71, <https://doi.org/10.1016/j.actbio.2019.08.042>.
- [68] D.S. Chong, B. Lindsey, M.J. Dalby, N. Gadegaard, A.M. Seifalian, G. Hamilton, Luminal surface engineering, 'micro and nanopatterning': potential for self endothelialising vascular grafts? *Eur. J. Vasc. Endovasc. Surg.* 47 (5) (2014) 566–576, <https://doi.org/10.1016/j.ejvs.2014.02.007>.
- [69] Q. Bian, J. Chen, Y. Weng, S. Li, Endothelialization strategy of implant materials surface: the newest research in recent 5 years, *J. Appl. Biomater. Funct. Mater.* 20 (2022) 22808000221105332, <https://doi.org/10.1177/22808000221105332>.
- [70] D. Hahn, D. Lee, W. Hyun, Y. Cho, C.H. Yoon, K.H. Jeon, S.H. Kang, T.J. Youn, I. H. Chae, Faster smooth muscle cell coverage in ultrathin-strut drug-eluting stent leads to earlier re-endothelialization, *Front. Bioeng. Biotechnol.* 11 (2023) 1207858, <https://doi.org/10.3389/fbioe.2023.1207858>.
- [71] Q. Guo, F. Huang, Y. Qing, S. Feng, X. Xiao, Y. Wang, M. Liang, T. Wang, W. E. Mitch, J. Cheng, Decreased Jagged1 expression in vascular smooth muscle cells delays endothelial regeneration in arteriovenous graft, *Cardiovasc. Res.* 116 (13) (2020) 2142–2155, <https://doi.org/10.1093/cvr/cvz333>.
- [72] K. Miyagawa, M. Shi, P.I. Chen, J.K. Hennigs, Z. Zhao, M. Wang, C.G. Li, T. Saito, S. Taylor, S. Sa, A. Cao, L. Wang, M.P. Snyder, M. Rabinovitch, Smooth muscle contract drives endothelial regeneration by BMP2-notch1-mediated metabolic and epigenetic changes, *Circ. Res.* 124 (2) (2019) 211–224, <https://doi.org/10.1161/circresaha.118.313374>.



- [73] J. Ren, T. Zhou, V.S.S. Pilli, N. Phan, Q. Wang, K. Gupta, Z. Liu, N. Sheibani, B. Liu, Novel paracrine functions of smooth muscle cells in supporting endothelial regeneration following arterial injury, *Circ. Res.* 124 (8) (2019) 1253–1265, <https://doi.org/10.1161/circresaha.118.314567>.
- [74] H. Miyachi, S. Tara, H. Nakayama, R. Hama, T. Sugiura, J.W. Reinhardt, T. Yi, Y. U. Lee, A.Y. Lee, S. Miyamoto, T. Shoji, Y. Nakazawa, C.K. Breuer, T. Shinoka, Transmural macrophage migration into an arterial bioresorbable vascular graft promotes inflammatory-mediated response and collagen deposition for vascular remodeling, *Acta Biomater.* 183 (2024) 146–156, <https://doi.org/10.1016/j.actbio.2024.05.055>.
- [75] L.M. Akyürek, L.C. Paul, K. Funa, E. Larsson, B.C. Fellström, Smooth muscle cell migration into intima and adventitia during development of transplant vasculopathy, *Transplantation* 62 (10) (1996) 1526–1529, <https://doi.org/10.1097/00007890-199611270-00029>.
- [76] B.N. Brown, J.E. Valentin, A.M. Stewart-Akers, G.P. McCabe, S.F. Badylak, Macrophage phenotype and remodeling outcomes in response to biologic scaffolds with and without a cellular component, *Biomaterials* 30 (8) (2009) 1482–1491, <https://doi.org/10.1016/j.biomaterials.2008.11.040>.
- [77] S.Y. Schubert, A. Benarroch, J. Ostvang, E.R. Edelman, Regulation of endothelial cell proliferation by primary monocytes, *Arterioscler. Thromb. Vasc. Biol.* 28 (1) (2008) 97–104, <https://doi.org/10.1161/atvbaha.107.157537>.
- [78] F. Zhang, M.W. King, Immunomodulation strategies for the successful regeneration of a tissue-engineered vascular graft, *Adv Healthc Mater* 11 (12) (2022) e2200045, <https://doi.org/10.1002/adhm.202200045>.
- [79] F. Copes, N. Pien, S. Van Vlierberghe, F. Boccafroschi, D. Mantovani, Collagen-based tissue engineering strategies for vascular medicine, *Front. Bioeng. Biotechnol.* 7 (2019) 166, <https://doi.org/10.3389/fbioe.2019.00166>.
- [80] Z. Wang, L. Liu, S.M. Mithieux, A.S. Weiss, Fabricating organized elastin in vascular grafts, *Trends Biotechnol.* 39 (5) (2021) 505–518, <https://doi.org/10.1016/j.tibtech.2020.09.003>.
- [81] D.V. Patel, T.J. Vachharajani, Principles of treating enlarging pseudoaneurysm in a dialysis arteriovenous graft, *Hemodial. Int.* 22 (1) (2018) E11–e14, <https://doi.org/10.1111/hdi.12588>.
- [82] D. Shemesh, I. Goldin, A. Verstandig, D. Berelowitz, I. Zahal, O. Olsha, Upper limb grafts for hemodialysis access, *J. Vasc. Access* 16 (Suppl 9) (2015) S34–S39, <https://doi.org/10.5301/jva.5000367>.
- [83] X. Qiu, B.L. Lee, S.Y. Wong, X. Ding, K. Xu, W. Zhao, D. Wang, R. Sochol, N. Dong, S. Li, Cellular remodeling of fibrotic conduit as vascular graft, *Biomaterials* 268 (2021) 120565, <https://doi.org/10.1016/j.biomaterials.2020.120565>.
- [84] L. Li, Y. Ma, G. He, S. Ma, Y. Wang, Y. Sun, Pilose antler extract restores type I and III collagen to accelerate wound healing, *Biomed. Pharmacother.* 161 (2023) 114510, <https://doi.org/10.1016/j.biopha.2023.114510>.
- [85] S. Matsuura, T. Takayama, T.G. Oyama, K. Oyama, M. Taguchi, T. Endo, T. Akai, T. Isaji, K. Hoshina, A radiation-crosslinked gelatin hydrogel that promotes tissue incorporation of an expanded polytetrafluoroethylene vascular graft in rats, *Biomolecules* 11 (8) (2021), <https://doi.org/10.3390/biom11081105>.
- [86] J.A. Cordero Jr., W.C. Quist, A.D. Hamdan, M.D. Phaneuf, M.A. Contreras, F. W. LoGerfo, Identification of multiple genes with altered expression at the distal anastomosis of healing polytetrafluoroethylene grafts, *J. Vasc. Surg.* 28 (1) (1998) 157–166, [https://doi.org/10.1016/s0741-5214\(98\)70211-3](https://doi.org/10.1016/s0741-5214(98)70211-3).
- [87] H. Wang, Y. Xiao, Z. Fang, Y. Zhang, L. Yang, C. Zhao, Z. Meng, Y. Liu, C. Li, Q. Han, Z. Feng, Fabrication and performance evaluation of PLLC-hCOLIII small-diameter vascular grafts crosslinked with procyanidins, *Int. J. Biol. Macromol.* 251 (2023) 126293, <https://doi.org/10.1016/j.ijbiomac.2023.126293>.
- [88] S.S. Ahn, H.I. Machleder, R. Gupta, W.S. Moore, Perigraft seroma: clinical, histologic, and serologic correlates, *Am. J. Surg.* 154 (2) (1987) 173–178, [https://doi.org/10.1016/0002-9610\(87\)90173-5](https://doi.org/10.1016/0002-9610(87)90173-5).
- [89] P.K. Lin, G.E. Davis, Extracellular matrix remodeling in vascular disease: defining its regulators and pathological influence, *Arterioscler. Thromb. Vasc. Biol.* 43 (9) (2023) 1599–1616, <https://doi.org/10.1161/atvbaha.123.318237>.
- [90] B. Kahle, C. Schmidtke, N. Hunzelmann, C. Bartels, H.H. Sievers, H. Steenbock, D. P. Reinhardt, J. Brinckmann, The extracellular matrix signature in vein graft disease, *Can. J. Cardiol.* 32 (8) (2016) 1008.e11–1008.e17, <https://doi.org/10.1016/j.cjca.2015.11.014>.
- [91] M. Rahmani, R.P. Cruz, D.J. Granville, B.M. McManus, Allograft vasculopathy versus atherosclerosis, *Circ. Res.* 99 (8) (2006) 801–815, <https://doi.org/10.1161/01.RES.0000246086.93555.f3>.